Analysis and Design of Interior Permanent Magnet Synchronous Motor Using a Sequential-Stage Magnetic Equivalent Circuit

Jae-Gil Lee[1], Dong-Kuk Lim[2], and Hyun-Kyo Jung[1]

[1]Department of Electrical and Computer Engineering, Seoul National University, Seoul 08826, South Korea
[2]School of Electrical Engineering, University of Ulsan, Ulsan 44610, South Korea

In the interior permanent magnet synchronous motor (IPMSM) design for the traction motor of fuel cell electric vehicles (FCEVs), it is necessary to analyze the nonlinear characteristics including saturation due to the requirement of a high torque density. The finite element method (FEM) is the most widely used technique for electric machine designs because complicated computations can be taken into account. However, a large amount of analysis over the entire design is a computationally large burden. To address this problem, this paper proposes a fast and accurate analysis method, sequential-stage magnetic equivalent circuit (SSMEC). The proposed method consists of no-load, q-axis circuit analysis, d-axis circuit analysis, and motor characteristic calculation. Because the proposed method can quickly and accurately analyze the complex shapes of an IPMSM, it can be used effectively throughout the entire motor design process. The effectiveness of the proposed SSMEC was verified in comparing with experimental results.

Index Terms—**Fuel cell electric vehicle (FCEV), interior permanent magnet (IPM) motor, magnetic equivalent circuit (MEC).**

I. Introduction

CONSIDERING the global issue of carbon dioxide emissions, fuel cell electric vehicles (FCEVs), which use hydrogen as an energy source to drive electric traction motors and emit only water, have attracted attention as a leading eco-friendly automobile for use in the near future [1]. The traction motor for an FCEV must be compact and light due to the limited mounting space. It must also have high-efficiency characteristics. In order to meet these requirements, interior permanent magnet synchronous motors (IPMSMs), which have high torque density, efficiency, and excellent mechanical stability, are suitable for FCEVs.

In the design of electric machines, the finite element method (FEM) and the magnetic equivalent circuit (MEC) method are widely used as analysis methods. The MEC simplifies the model as lumped-parameters and analyzes it rapidly [2]. However, there are limitations in analyzing nonlinear characteristics with magnetic saturation in an iron core when these methods are applied to high torque density designs such as the IPMSM for an FCEV. Specifically, it is quite difficult to accurately analyze the load condition with a high degree of magnetic saturation. In this regard, the FEM is generally used for an accurate analysis of an IPMSM. However, there is a considerable computation during such an analysis through the FEM in the overall design process.

To address this problem, we propose a sequential-stage MEC (SSMEC) which takes the magnetic saturation effect in the iron core, the slotting effect, and the on-load characteristics of IPMSMs into account. Specifically, the proposed method is very powerful in the early design stage as it effectively grasps the general properties of the motor, such as the characteristic curve, the back electromotive force (EMF), and the total harmonic distortions (THDs).

The proposed MEC is divided into no-load, d-axis, and q-axis circuits. First, the no-load equivalent circuit derives the no-load characteristics considering the slotting effects by modeling the magneto motive force (MMF) source, the leakage magnetic flux source, and the conformal mapping method referring to the previous studies [3], [4]. Then, in the d- and q-axis equivalent circuit analysis, the accuracy is improved by sequentially utilizing the results of the no-load analysis. In order to reflect the saturation effects of the iron core in the load analysis, the B–H data of the actual iron core is utilized in an iterative process in the iron core reluctance calculations.

Finally, in this paper, the proposed method is applied to the design of an IPMSM for an FCEV and the validity of the proposed method is verified through a comparison with the experimental results of a prototype model.

II. Target IPMSM for FCEV

Table I shows the design limitations and requirements of the IPMSM for the target FCEV. The IPMSM uses a rare-earth magnet material with high remanence and a high current density to ensure a high power density in a limited space. Hence, the IPMSM is inevitably designed with high magnetic saturation, and the accurate nonlinear analysis is necessary using actual material data of the iron core. Also, as shown in Fig. 1, a multi-segmented and multi-layered (MSML) type of rotor structure is used. It shows excellent performance and structural characteristics and is easy to manufacture. However, the MSML rotor type IPMSM requires complicated analyses due to the numerous design variables and high design freedom. This causes a considerable amount of analysis with numerous trial and error designs. Hence, this paper proposes SSMEC for a fast and accurate analysis and utilizes it during the IPMSM design process for an FCEV. Meanwhile, this target model operates with a highly saturated iron core, where the maximum

Manuscript received November 3, 2018; revised January 4, 2019; accepted June 6, 2019. Date of publication July 2, 2019; date of current version September 18, 2019. Corresponding author: D.-K. Lim (e-mail: ldk8745@ulsan.ac.kr).

Color versions of one or more of the figures in this article are available online at http://ieeexplore.ieee.org.

Digital Object Identifier 10.1109/TMAG.2019.2922043

TABLE I
SPECIFICATION OF THE TARGET TRACTION IPMSM FOR AN FCEV

Items	Values
No. of Poles / Slots / Phases	6 /27/ 3
Stator outer /inner diameter (mm)	240 /172
Axial length (mm)	230
Airgap length (mm)	1
Rotor outer /inner diameter (mm)	170 /50
Rated torque (Nm)	300
Rated current (Arms)	360
DC link voltage (V)	240

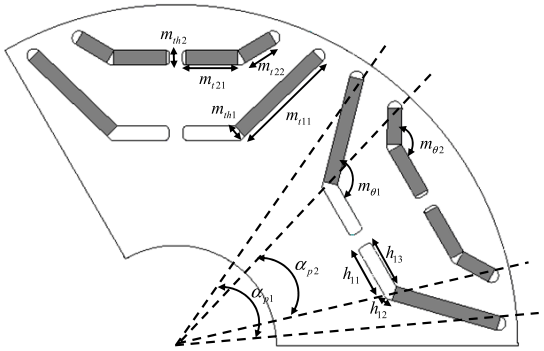

Fig. 1. Rotor configuration and design variables of the target IPMSM.

level of magnetic flux density in the maximum torque angle exceeds 1.8 T.

III. PROPOSAL OF THE SEQUENTIAL STAGE MAGNETIC EQUIVALENT CIRCUIT

To simplify load analysis of the IPMSM motor, the problem can be conducted by two analyses, which are d-axis and q-axis as defined by the pole direction of the permanent magnet and the direction electrically 90° away from the d-axis [4]. Accordingly, the SSMEC technique proposed in this paper consists of the four steps of no-load analysis, d-axis analysis, q-axis analysis, and motor characteristics calculations. First, the no-load analysis is conducted, after which the results of the no-load analysis are used for the load analysis, with the nonlinear characteristics of the iron core reflected by applying actual B–H data to an iterative calculation routine. Finally, the characteristics of the motor, in this case, the torque at each current phase angle and the terminal voltage, can be calculated through a combination of the no-load and load results. Detailed descriptions of each step are given below.

A. Step 1: No-Load Analysis (Magnet Excitation)

First, referring to the previous research [3], the no-load analysis is conducted while only considering the excitation condition by the permanent magnets. First, a MEC without slotting effects of the stator is constructed. The configuration of the MEC regards the permanent magnet and air gap flux path as the magnetic flux source and the air gap reluctances, respectively. In addition, the center posts and bridges of the rotor which usually operate under high saturation are developed as fixed leakage magnetic flux sources with air reluctances values. The air gap flux density can then be derived

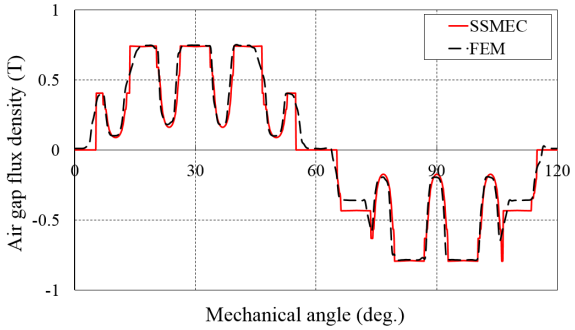

Fig. 2. Comparison of air gap flux density by SSMEC and FEM with magnet excitation.

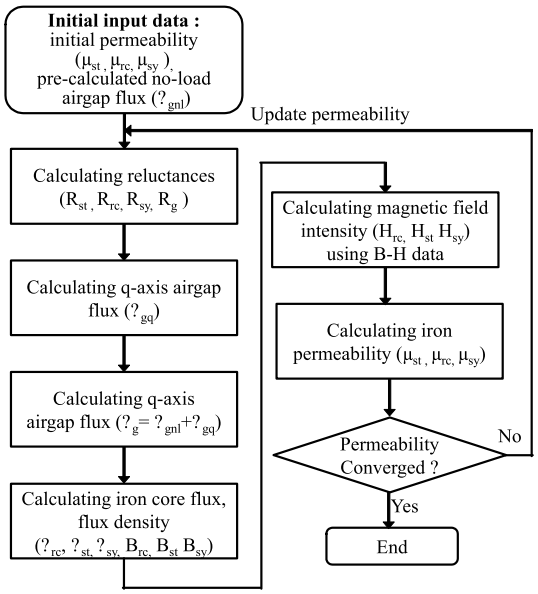

Fig. 3. Overall flowchart of step 2: q-axis analysis.

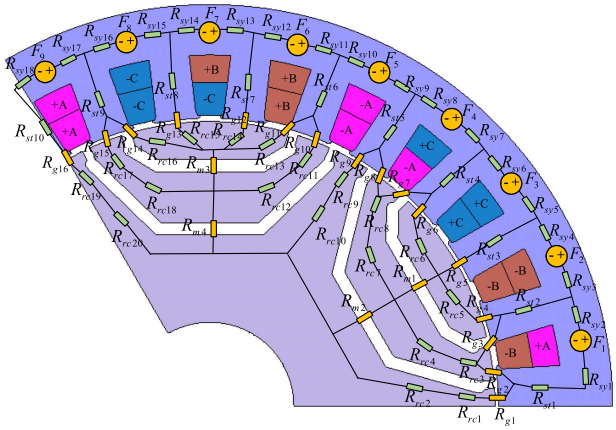

Fig. 4. Q-axis analysis model of the target IPMSM.

by solving the developed equivalent circuit with slotting effects finally reflected by a conformal mapping technique [5]. The finally calculated no-load air gap flux density for the target FCEV traction motor model is compared with the FEM analysis results shown in Fig. 2.

B. Step 2: q-Axis Analysis (Current Phase Angle = 0°)

When an armature current is applied to the IPMSM, a flux path on the q-axis arises by bypassing the permanent magnet.

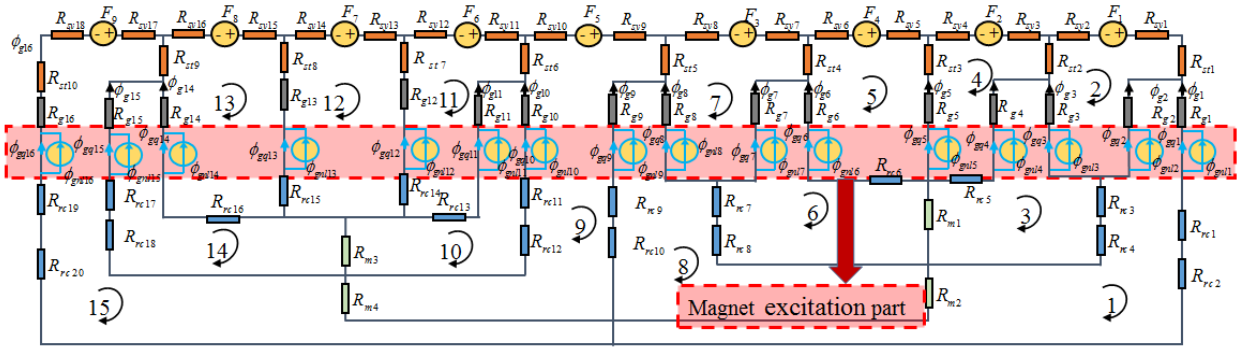

Fig. 5. MEC of the MSML IPMSM reflecting the permanent magnet excitation and q-axis current excitation.

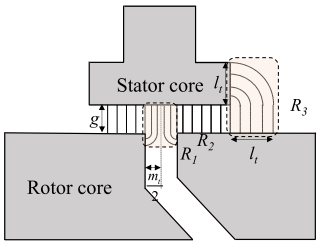

Fig. 6. Air gap reluctance model considering flux paths of slot side and magnet end part.

Consequently, the total reluctance is low such that a large amount of magnetic flux is formed and the degree of saturation in the iron core is high. Hence, it is very important to accurately estimate the reluctance values of the iron core. Moreover, the coupling effect of the magnetic flux formed by the permanent magnet should be considered in the q-axis analysis. Fig. 3 shows an overall flowchart for analyzing the q-axis MEC which is graphically modeled in Fig. 4. During q-axis excitation, the center post and the bridge of the rotor are completely saturated and the permanent magnets can be magnetically regarded as air. Hence, they can be replaced with air, as shown in Fig. 4. Detailed processes are as follows.

First, the air gap magnetic flux is calculated from the results in step 1 and the initial permeability of the iron cores, which are required to reflect the permanent magnet excitation in armature excitation model and to start the iterative routine.

Next, the reluctances of the iron core, air gap, and magnet are calculated using the shape parameters, after which the air gap flux density is calculated by solving the circuit equations of the MEC in Fig. 5 with the applied q-axis MMF. The highlighted box in Fig. 5 represents the magnetic flux sources in the air gap which result from the previous no-load analysis. These flux sources are summed with the air gap flux resulting from the calculation of the q-axis excitation sources.

Specifically, as shown in Fig. 6, the air gap reluctances are defined not only by the magnetic flux path formed directly through the stator tooth to the rotor iron core but also by the path bypassing the slot shoe side and the flux path through the magnet end parts. These magnetic flux paths are considered as two additional air gap reluctances $R_{\rm sg} = l_{\rm seff}/\mu A_{\rm sg}$ and $R_{\rm mg} = l_{\rm meff}/\mu A_{\rm mg}$, where $l_{\rm seff}$ and $l_{\rm meff}$ correspondingly represent the each of effective flux path calculated by (1), (2). Here, g, l_t, and m_t represent the air gap length, the thickness of the slot shoe side, and magnet thickness, respectively. We assumed that the flux path is formed as straight lines through the air gap part and as the arc lines through the teeth side and magnet end parts. To obtain the average value of the effective length, we divided the flux path into sufficiently large N. Finally, the parallel air gap reluctances can be summed as R_g

$$l_{\rm seff} = g + \frac{1}{N}\sum_{i=1}^{N}\frac{\pi}{2}\frac{l_t}{N}i \tag{1}$$

$$l_{\rm meff} = g + \frac{1}{N}\sum_{i=1}^{N}\frac{\pi}{2}\frac{m_t}{2N}i. \tag{2}$$

The calculated air gap flux density reflects both the effects from the permanent magnets and the q-axis current. However, it is necessary to consider the saturation effects of the iron core. To consider the saturation effects, we utilize the actual B–H data of the iron core. The magnetic flux density at the iron core is calculated using the summed air gap flux density, after which the permeability $\mu_{\rm st}$, $\mu_{\rm rc}$, and $\mu_{\rm sy}$ can be calculated with the relationships $\mu_{\rm st} = B_{\rm st}/H_{\rm st}$, $\mu_{\rm rc} = B_{\rm rc}/H_{\rm rc}$, and $\mu_{\rm sy} = B_{\rm sy}/H_{\rm sy}$. Using this permeability value again, we return to the calculation step of the iron core reluctance. This iterative routine continues until the change rate of the permeability values in the present iteration and the previous iteration converges very little with the relationship $\varepsilon = (\mu_{c(i+1)} - \mu_{ci})/\mu_{ci}$. Here, μ_{ci} is the relative permeability of the iron core calculated in the ith iteration.

C. Step 3: d-Axis Analysis (Current Phase Angle = 90°)

An IPMSM can be operated in a wide speed region by a flux weakening operation utilizing the d-axis current. Unlike the q-axis, the flux path of the d-axis excitation contains considerable reluctance because the flux path is formed directly through the permanent magnet, which brings about low magnetic saturation of the iron core. Therefore, it is possible simply to analyze the magnetic circuit without considering the saturation effects of the iron core. Fig. 7 shows the d-axis circuit model of the target IPMSM. The d-axis circuit model includes several reluctances of the air gap and flux

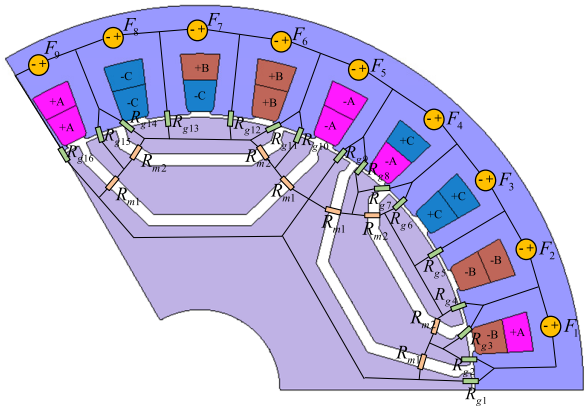

Fig. 7. D-axis analysis model of the target IPMSM.

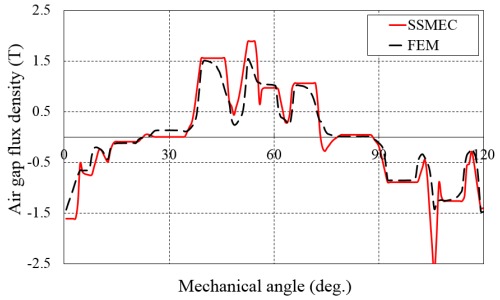

Fig. 8. Comparison of air gap flux density by SSMEC and FEM at maximum torque operation where the current phase angle is 45°.

path through the magnet and the MMF source of the d-axis armature current.

D. Step 4: Motor Performance Calculation

In this step, the motor performances are calculated using the field results from the previous steps. The flux linkage can be calculated by summing the air gap flux density according to the winding pattern. Subsequently, the flux linkages can be converted to the d- and q-coordinate systems through transformation formulas to calculate the steady-state motor characteristics (3)–(6). Here, T_{ave}, V_d, V_q, and V_T represent the average torque, the d-axis voltage, the q-axis voltage, and the terminal voltage, respectively. Moreover, we can calculate the back EMF, THD, torque-speed curve, torque per phase angle, and terminal voltage as well.

$$T_{\text{ave}} = \frac{3}{2}\frac{N_p}{2}(\lambda_d i_q - \lambda_q i_d) \tag{3}$$

$$V_d = R_s i_d - \omega_r \lambda_q \tag{4}$$

$$V_q = R_s i_q + \omega_r \lambda_d \tag{5}$$

$$V_T = \sqrt{V_d^2 + V_q^2}. \tag{6}$$

IV. Result and Verification

In order to confirm the validity of the proposed SSMEC, the finally calculated air gap flux density result under a continuous rating is compared with the FEM analysis results in Fig. 8. The difference occurs in a few regions such as around 5°, 45°, 55°, 70°, and 105°, which are seriously saturated regions with q-axis current and permanent magnet. Despite the difference, it shows sufficient accuracy and is thus feasible for use in the early stages of the motor design.

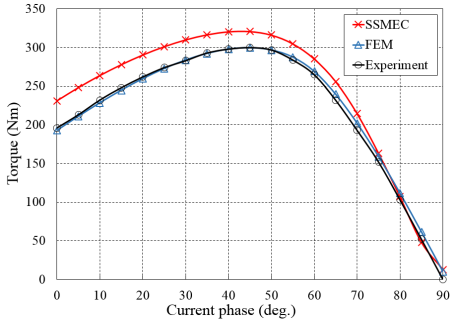

Fig. 9. Torque comparison at each current phase angle according to SSMEC, FEM, and the experimental data.

Finally, the motor performance calculated by the SSMEC method is verified through a comparison with the FEM analysis results and the experimental data of an actually designed FCEV motor. Fig. 9 shows the torque at each current phase angle. The results from the proposed SSMEC and the experimental values are 320.8 and 300 Nm, respectively, therefore showing approximately 7% error at a maximum torque angle of 45°. In addition, the accuracy increases as the phase angle increases. The reason is that the degree of saturation in the iron core significantly increases as the magnitude of q-axis current increases. In the viewpoint of calculation time, it takes several tens of seconds to derive the torque per phase angle curve in Fig. 9, but the FEM requires about an hour.

V. Conclusion

This paper contributes to the SSMEC method with rapid and accurate analysis of an MSML type IPMSM. In particular, not only the no-load but also the load characteristics, including magnetic saturation and the coupling effects, can be analyzed based on actual material data. Hence, the proposed SSMEC is available for wide use in various IPMSM designs with high magnetic saturation effects requiring high torque density.

Acknowledgment

This work was supported by the National Research Foundation (NRF) of Korea grant funded by the Korea Government (Ministry of Science and ICT) (2017R1C1B5077038).

References

[1] T. Hasegawa, H. Igarashi, and K. Gemba, "Creation of FCEV market: A new approach to the emerging economy of self-sustainability," in *Proc. IEEE Int. Conf. Ind. Eng. Eng. Manage.*, Bangkok, Thailand, Dec. 2013, pp. 1344–1347.

[2] M. Cheng, K. T. Chau, C. C. Chan, E. Zhou, and X. Huang, "Nonlinear varying-network magnetic circuit analysis for doubly salient permanent-magnet motors," *IEEE Trans. Magn.*, vol. 36, no. 1, pp. 339–348, Jan. 2000.

[3] D.-K. Lim *et al.*, "Analysis and design of a multi-layered and multi-segmented interior permanent magnet motor by using an analytic method," *IEEE Trans. Magn.*, vol. 50, no. 6, Jun. 2014, Art. no. 8201308.

[4] M. N. Uddin and M. A. Rahman, "High-speed control of IPMSM drives using improved fuzzy logic algorithms," *IEEE Trans. Ind. Electron.*, vol. 54, no. 1, pp. 190–199, Feb. 2007.

[5] K. Boughrara, R. Ibtiouen, D. Zarko, O. Touhami, and A. Rezzoug, "Magnetic field analysis of external rotor permanent-magnet synchronous motors using conformal mapping," *IEEE Trans. Magn.*, vol. 46, no. 9, pp. 3684–3693, Sep. 2010.